ARTICLE

OPEN

Check for updates

Dichotomy between freshwater and heat flux effects on oceanic conveyor belt stability and global climate

Aixue Hu [1✉], Gerald A. Meehl [1], Ayako Abe-Ouchi [2], Weiqing Han [3], Bette Otto-Bliesner [1], Feng He [4], Tongwen Wu [5], Nan Rosenbloom [1], Warren G. Strand [1] & James Edwards[1]

The Atlantic meridional overturning circulation is an important global-scale oceanic circulation, and its changes may be responsible for past abrupt climate change events. By using two versions of a coupled climate model, here we show that the stability of this circulation depends not only on the background climate, but also on the type of primary external forcing: freshwater vs. greenhouse gases. When freshwater forcing is dominant, hysteresis of this circulation (an abrupt collapse/reactivation) becomes possible only under simulated glacial conditions with closed Bering Strait. Under present day and future conditions, both freshwater and greenhouse gas forcings could collapse this circulation, but only greenhouse gas forcing produced a bi-stable equilibrium state comparable to abrupt climate change. Our results demonstrate that the Bering Strait status (open vs. closed) may facilitate or prohibit the existence of this circulation's hysteresis, irrespective of the background climate conditions, but is directly related to the primary forcing.

[1] Climate and Global Dynamics Laboratory, National Center for Atmospheric Research, Boulder, CO 80307, USA. [2] Atmosphere and Ocean Research Institute, University of Tokyo, Kashiwa 277-8568, Japan. [3] Department of Atmospheric and Oceanic Sciences, University of Colorado, Boulder, CO 80301, USA. [4] Center for Climatic Research, Nelson Institute for Environmental Studies, University of Wisconsin-Madison, Madison, WI, USA. [5] Beijing Climate Center, Chinese Administration of Meteorology, 100081 Beijing, China. ✉email: ahu@ucar.edu

Multiple proxy records suggest frequent abrupt climate change events during the last glacial period, identified as Heinrich[1,2] and Dansgaard–Oeschger events[3–5], but a near absence of such events during the Holocene[6,7]. While hysteresis in the Atlantic meridional overturning circulation (AMOC or the global conveyer belt)[8–10] has been demonstrated to be capable of inducing global scale climate changes in which AMOC can suddenly collapse or reactivate in relation to slow changes in external thermohaline forcing[11–14], it is still a challenge to show whether AMOC's hysteresis exists in climate conditions of present-day or the next few centuries. Yet, recent studies suggest that the current state of AMOC might be the weakest in the last millennium[15] and this could be signs of AMOC going towards collapse[16].

Traditionally, analysis of AMOC stability has focused primarily on the freshwater runoff into the North Atlantic from melting ice sheets[10,17–19] because changes in heat flux due to changes of greenhouse gases (GHGs) were relatively smaller and the change rate is much slower. For example, carbon dioxide (CO_2) concentration varied between ~180 and 280 parts per million by volume (ppmv) for the last million years before industrialization. The CO_2 change of this magnitude took at least 10 thousand years[7]. Correspondingly the change in global mean sea level was in the order of 100 meters in the same timeframe[20] with a peak rate equivalent of ~20-m global mean sea level rise in 350 years during meltwater pulse 1A[21]. However, studies also suggest that under the rapid and unprecedented increase in GHG concentration in recent decades and the near future, AMOC is expected to weaken due primarily to GHG-induced heating[22,23]. Although explorations of mass losses from Greenland and Antarctic Icesheets under global warming have also been carried out, results suggest that unless Greenland Icesheet melting far exceeds reasonable projections, this melt water from Greenland will not dramatically induce an accelerated AMOC slowdown on top of the GHG forcing[19,24–27].

Either freshwater or GHG-induced heat flux changes can independently affect the oceanic stratification in the subpolar North Atlantic where the deep convection occurs; therefore, it is important to isolate how these two factors may have influenced the AMOC stability in the past, and to project their influence under present and future climate conditions. To do this, we have conducted a series of simulations under different climate conditions using the Community Climate System Model versions 3 and 4 (CCSM3 and CCSM4, see method section for details)[28,29]. These simulations represent mid-glacial (15 thousand years before present day, 15ka), modern (1990AD), and future climate conditions (the representative concentration pathway 8.5 or RCP8.5 scenario).

To test the effects of freshwater flux as the primary external forcing on AMOC, we have conducted one paired simulation for mid-glacial and two paired simulations for modern conditions that consider whether the Bering Strait is open (bso) or closed (bsc) within each pair using CCSM3. The difference between two paired simulations under modern conditions is the rate of the freshwater forcing: 200 m^3 s^{-1}year^{-1} increment (fast rate, F) vs. 100 m^3 s^{-1}year^{-1} increment (slow rate, S) (see Table 1, Supplementary Fig. 1a–c, and method section for details of the experimental design and naming convention). The difference between the paired simulations under different background climate conditions is the region where the freshwater is added: subtropical Atlantic (20–50°N) for modern conditions vs. subpolar North Atlantic (50–70°N) for mid-glacial conditions with freshwater increment rate of 100 m^3 s^{-1}year^{-1}. The design of these three paired experiments partially follows two previous studies[12,30]. Hereafter these experiments are referred to as Mid-glacial, ModernF, and ModernS.

To test the effects of GHG-induced heat flux change as the primary forcing on AMOC, a numerical simulation branched from the preindustrial control simulation using CCSM4 is carried out and forced by historical all known external forcings (e.g., GHGs, solar radiation, and aerosols) from 1850 to 2005. From 2006-2300, this experiment adopts the RCP8.5 scenario and then we keep all forcings at year 2300AD RCP8.5 levels for 2301-2600AD to allow the AMOC and surface climate to reach a quasi-equilibrium state with the GHG forcing. These forcings are then reversed back to the preindustrial level for years 2601-3050AD

Table 1 Experiments and background conditions.

Case	model	background	Bering Strait	Length (year)	CO_2 (ppmv)	Annual Freshwater change (m^3 s^{-1}year^{-1})	Area where freshwater is added in North Atlantic
ModernF-bso	CCSM3	1990	open	4400	355	200	20–50°N
ModernF-bsc	CCSM3	1990	closed	4200	355	200	20–50°N
ModernS-bso	CCSM3	1990	open	8800	355	100	20–50°N
ModernS-bsc	CCSM3	1990	closed	8800	355	100	20–50°N
Mid-glacial-bso	CCSM3	15 ka BP	open	3000	214	100	50–70°N
Mid-glacial-bsc	CCSM3	15 ka BP	closed	3000	214	100	50–70°N
FutureGHG	CCSM4	Historical/RCP8.5	open	1200	280–1950	0	–
MGbsc_600	CCSM3	15 ka BP	closed	340	214	60000 fixed	50–70°N
MGbsc_700	CCSM3	15 ka BP	closed	400	214	70000 fixed	50–70°N
MGbsc_900	CCSM3	15 ka BP	closed	400	214	90000 fixed	50–70°N
MGbsc_2100	CCSM3	15 ka BP	closed	400	214	90000 fixed	50–70°N
MGbsc_2300	CCSM3	15 ka BP	closed	400	214	70000 fixed	50–70°N
GHG_1000u	CCSM4	RCP8.5	open	200	1000	0	–
GHG_1100u	CCSM4	RCP8.5	open	200	1100	0	–
GHG_1200u	CCSM4	RCP8.5	open	200	1200	0	–
GHG_1000d	CCSM4	RCP8.5	open	200	1000	0	–
GHG_1100d	CCSM4	RCP8.5	open	200	1100	0	–
GHG_1200d	CCSM4	RCP8.5	open	200	1200	0	–

ModernF=modern background conditions with fast freshwater forcing changes (200 m^3 s^{-1}year^{-1}). ModernS=modern background conditions with slow freshwater forcing changes (100 m^3 s^{-1}year^{-1}), and Mid-glacial or MG represents mid-glacial background conditions with a rate of freshwater forcing changes (100 m^3 s^{-1}year^{-1}). "bso" represents open Bering Strait conditions and "bsc" represents closed Bering Strait conditions. FutureGHG represents the simulation using historical and RCP8.5 forcings. GHG represents greenhouse gas, and "u" or "d" represent the GHG increasing or decreasing phase. The numbers after MGbsc represent the year that the simulation is branched from the Mid-glacial-bsc experiment and the numbers after GHG represent the level of CO_2 in ppmv which are stabilized at.

(Supplementary Fig. 1d). Although all known forcings vary with time in this experiment, the changes of the AMOC and global climate are primarily caused by GHGs-induced radiative heating changes (note that there is no interactive ice sheet model here), especially for the periods using RCP8.5 scenario (2006-2895)[31]. Hereafter this simulation is called FutureGHG (for more details, see method section and Table 1).

In short, three paired experiments are used to test primarily how freshwater flux alone affects the AMOC hysteresis under different background mean states (mid-glacial vs. modern) and different geographic setups (open vs. closed Bering Strait), while the FutureGHG experiment is used to test primarily how GHG-induced heating will influence the AMOC hysteresis. Here, the changes in temperature and other climate variables in the three paired experiments are viewed as responses to the AMOC changes due to freshwater forcing. The changes in the hydro-logical cycle in the FutureGHG experiment are considered as responses to AMOC changes due to GHGs. Therefore, we define the AMOC stability in the first three paired experiments as freshwater-induced AMOC hysteresis and that in the FutureGHG experiment as the GHG-induced AMOC hysteresis.

Results

Freshwater vs. GHG forced AMOC hysteresis. Under mid-glacial condition (Fig. 1a; Supplementary Fig. 2a), the response of AMOC is more like a hysteresis with a closed Bering Strait (Mid-glacial-bsc, black and red lines) than that with a hypothetical open Bering Strait (Mid-glacial-bso, blue and green lines; note that arrows pointing to the direction of freshwater changes). For example, AMOC collapses rapidly from ~13 Sv (Sverdrup, $1 \, Sv \equiv 10^6 \, m^3 \, s^{-1}$) to 5 Sv (black line in Fig. 1a) when freshwater forcing changes from 0.06 Sv to 0.09 Sv, followed by a rapid AMOC recovery from ~8 Sv to 15 Sv when freshwater forcing declines from 0.09 Sv to 0.06 Sv (red line) with a closed Bering Strait. However, in the hypothetical open Bering Strait simulation under mid-glacial conditions (Mid-glacial-bso), the AMOC declines only 3 Sv (blue line) or increases 4 Sv (green line) for the same freshwater changes which is about 50% of those changes in Mid-glacial-bsc.

To quantify the AMOC changes further, running piecewise linear trends of AMOC are calculated for these two simulations (Fig. 2a and Supplementary Fig. 3a). Two methods are used for these running piecewise linear trends: (1) AMOC changes vs. freshwater flux changes with a freshwater running window of 0.008 Sv; (2) AMOC changes vs. time with a running time window of 300 years. The maximum rate of AMOC's decline in Mid-glacial-bsc is more than twice as large as that in Mid-glacial-bso (2.49 vs. 1.17 Sv$(\Delta 0.01 \, Sv)^{-1}$; $(\Delta 0.01 \, Sv)^{-1}$ represents a freshwater change of 0.01 Sv) during the freshwater flux increasing phase, but about 1.5 times of that in Mid-glacial-bso (1.92 vs. 1.27 Sv$(\Delta 0.01 \, Sv)^{-1}$) during the freshwater flux decreas-ing phase (with statistical significance of 95%). This further demonstrates that the changes in AMOC are more abrupt in Mid-glacial-bsc than in Mid-glacial-bso. Similar results can also be found when AMOC trends are calculated against time (Supple-mentary Fig. 3a). Moreover, the correlation coefficient between AMOC and freshwater flux is 0.79 for Mid-glacial-bsc, but 0.95 for Mid-glacial-bso. This indicates a nearly perfect linear relationship for Mid-glacial-bso between AMOC and freshwater changes, which means the changes in AMOC follow the changes of freshwater forcing without any delay (hysteresis) and this implies an absence of AMOC hysteresis (or abrupt AMOC transition) in Mid-glacial-bso. However, the AMOC variations in Mid-glacial-bsc more closely resembles the results in reference [12] (hereafter referenced as GR2001) which shows abrupt transitions

of AMOC and a delayed response to the freshwater forcing changes (Fig. 1a, e; for the mechanisms of the Bering Strait's influence on AMOC, see Supplementary Note 1).

To further test the AMOC stability under mid-glacial conditions with a closed Bering Strait, freshwater forcing is stabilized at different levels specified at 0.06 Sv, 0.07 Sv and 0.09 Sv for AMOC decreasing and increasing phases, respectively (see method section and Table 1 for more details). As shown in Fig. 3a, b and Supplementary Fig. 4a, the AMOC continuously declines and produces much weaker states (black triangles in Fig. 1a) even though the freshwater forcing is kept constant during AMOC decline phase. During AMOC strengthening phase, AMOC ends up in bit stronger states with stabilized freshwater forcing (red circles in Fig. 1a). On the one hand, this is a compelling demonstration that the AMOC has different quasi-equilibrium states under the same freshwater forcing with a closed Bering Strait under Mid-glacial conditions; on the other hand, this AMOC hysteresis is atypical since the recovery loop of AMOC is on top of collapsing loop, and will be discussed more later.

Under modern conditions, AMOC displays a more obvious hysteresis with a hypothetically closed Bering Strait (Fig. 1b, c, Supplementary Fig. 2b, c; black and red lines) regardless of the strength of changes in freshwater forcing rates, but a more linear relationship between AMOC and freshwater changes with an open Bering Strait (blue and red lines). By comparing ModernF-bsc with ModernS-bsc, the transition of the AMOC from active to collapse (or vice versa) is much sharper with a slower freshwater change rate than that with a faster rate of the freshwater changes. The maximum piecewise linear trend between AMOC and freshwater changes is 1.10 vs. 0.85 Sv$(\Delta 0.01 \, Sv)^{-1}$ (or ~30% higher) during AMOC collapsing phase for the slow vs. fast freshwater forcing change rates, respectively, but 2.14 vs. 1.98 Sv$(\Delta 0.01 \, Sv)^{-1}$ (or 8% higher) during AMOC reactivate phase (Figs. 2b, c, blue lines). This strongly implies that if the rate of freshwater change were slow enough to keep the AMOC at an equilibrium state with the freshwater forcing, this AMOC transition could become even more abrupt. This makes the coupled model results agree much better with previous results using Earth system model with intermediate complexity model with a freshwater forcing change at a 50% rate of the ModernS experiments[12,30,32], e.g., the black–red curve of Fig. 1c is much more like that of Fig. 1f (GR2001). A discussion of the AMOC hysteresis loop width is in Supplementary Note 2.

With a realistic open Bering Strait under modern conditions (ModernF_bso and ModernS_bso), the maximum piecewise linear trend between AMOC and freshwater forcing is only 0.44/0.62 Sv$(\Delta 0.01 \, Sv)^{-1}$ for ModernF_bso and 0.49/0.64 Sv$(\Delta 0.01 \, Sv)^{-1}$ for ModernS_bso during AMOC collapse/reactivate phase (Fig. 2b, c black lines). These numbers are only about 50% (30%) of those in the closed Bering Strait simulations during AMOC collapse (reactivate) phase and they are statisti-cally different from those in the closed Bering Strait simulations at 95% level. The linear correlation coefficients between AMOC and freshwater change are 0.97 for ModernS-bso and 0.96 for ModernF-bso, indicating that the relationship between AMOC and freshwater changes is slightly more linear for ModernS-bso than ModernF-bso (Fig. 1b-c; Supplementary Fig. 2b, c; blue and green lines). The corresponding correlation coefficients for the closed Bering Strait simulations are 0.87 for ModernS-bsc and 0.82 for ModernF-bsc, and both are much lower than those in the open Bering Strait simulations.

For future climate conditions, it has been projected that a continuous increase in atmospheric GHG concentration will result in a decline in AMOC strength[33-36], implying that GHG-induced heating effects would be the major contributor to the
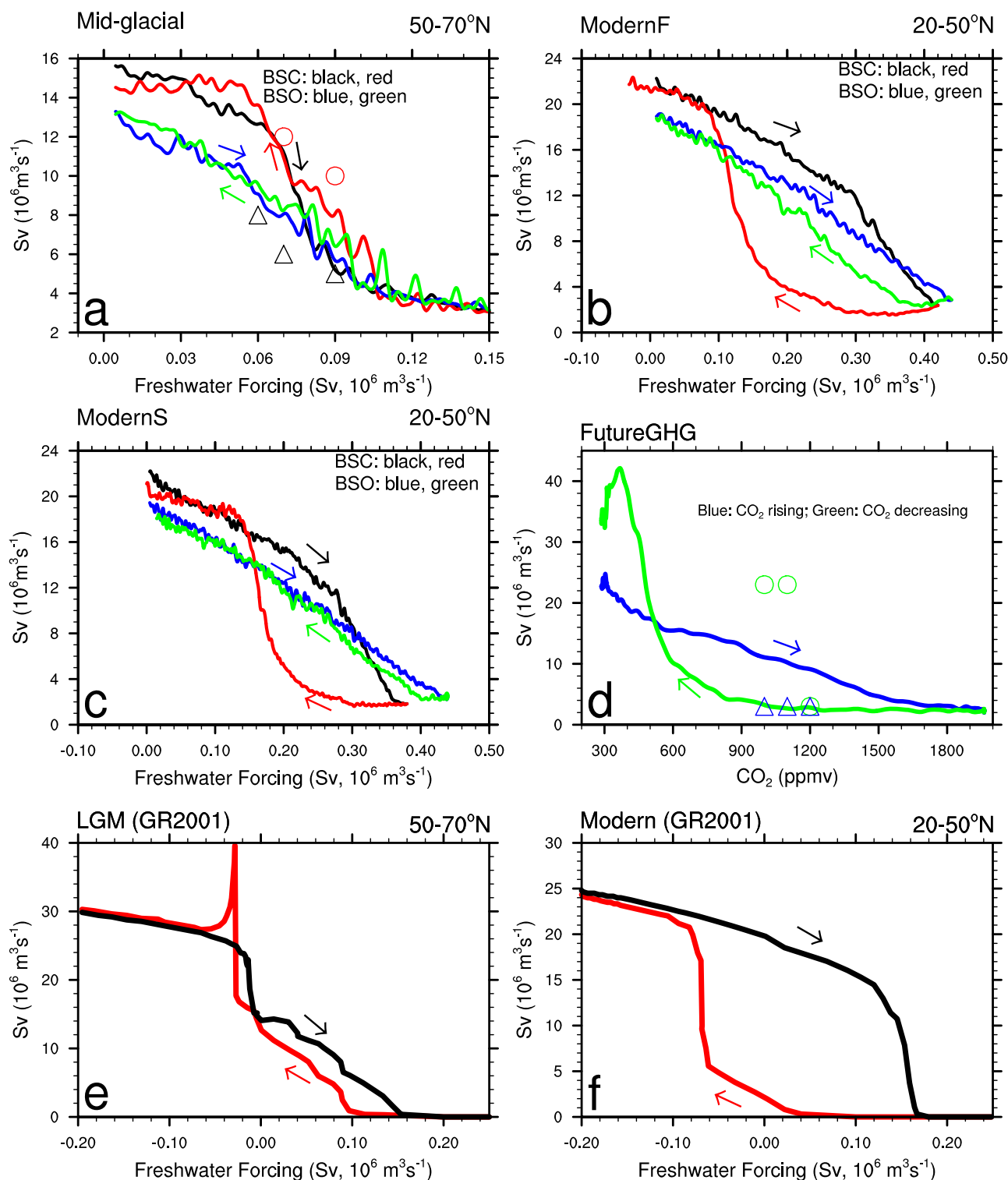
AMOC stability[22,23]. Under GHG forcing alone, AMOC declines quickly with a CO_2 concentration above 300 ppmv and collapses completely with CO_2 beyond 1500 ppmv in FutureGHHG (Fig. 1d; Supplementary Fig. 2d, blue line). As CO_2 forcing declines, AMOC stays at the collapsed state until CO_2 concentration is below 900 ppmv, then AMOC starts to recover slowly, but this recovery speeds up when CO_2 concentrations dip below 600 ppmv and quickly overshoots the initial AMOC strength by almost 100% due primarily to salt advection feedback[21,37–39] (green line). During the AMOC declining phase, a large decline

rate of ~1.8 Sv(10 ppmv CO_2)$^{-1}$ occurs in 1920s and weakens afterward (Fig. 2d). However, in respect to time, the largest rate of AMOC decline appears around 2130 (~0.15 Sv year^{-1}; Supplementary Fig. 3d). During the AMOC recovery phase, the rate of AMOC increase reaches a maximum of ~1.8 Sv(10 ppmv CO_2)$^{-1}$ in early 2870 s, which occurs almost at the same time when the rate is measured with respect to time (Fig. 2d vs. Supplementary Fig. 3d).

For RCP8.5 scenarios, the stabilized CO_2 concentration is 1962 ppmv. The AMOC stays in the off-mode for a total of 550 years

Fig. 1 The AMOC hysteresis due to freshwater and GHG forcings. a AMOC hysteresis loop under mid-glacial climate conditions (15 ka before present day) with an open (BSO) and closed (BSC) Bering Strait and freshwater is added between 50 and 70ºN to the Atlantic (Mid-glacial); (**b**) the same as (**a**) but under modern climate conditions (1990AD) and freshwater is added between 20 and 50ºN to the Atlantic (ModernF); (**c**) the same as (**b**), but with an annual freshwater increment at 50% of that in (**b**) (ModernS); (**d**) AMOC hysteresis loop due to changes in greenhouse gas forcing (from 285 to 1962 ppmv; FutureGHG); (**e**) and (**f**) are partially adopted from Fig. 1a, b in ref. [12] and labeled as GR2001. Here we only included the AMOC hysteresis loop under last glacial maximum (LGM) conditions with freshwater being added into 50–70ºN of the Atlantic (**e**) and under modern conditions with freshwater being added into 20–50ºN of the Atlantic (**f**) in order to make these two panels comparable to (**a**–**c**). For (**a**–**c**), back/red lines are for closed Bering Strait simulations and blue/green lines for open Bering Strait simulations, and black/blue lines are the freshwater increasing phase and red/green lines for freshwater decreasing phase. Blue/green lines in (**d**) represent the greenhouse gas increasing/decreasing phase. For (**e**, **f**) which is created using data from Ganopolski and Rahmstorf[12], black line represents the freshwater flux increase phase and red line the decrease phase. To partially adapt Fig. 1a, b from ref. [12], we used an online digitizer tool called "WebPlotDigitizer" (https://automeris.io/WebPlotDigitizer/) which is a free online software. The arrows indicate the direction of the freshwater or GHG changes, such that the arrows pointing right and down are for freshwater or GHG increasing phase and the arrows pointing left and up are for freshwater or GHG decreasing phase. The color of the arrows matches the color of the lines. The triangles and circles in Figs. 1a and d represent the quasi-equilibrium state of AMOC under different stabilized freshwater or CO_2 levels in the sensitivity experiments (see Table 1 and the method section for details). The triangles represent the AMOC states in rising freshwater or CO_2 phase and the circles represent the AMOC states in decreasing freshwater or CO_2 phase, and the color of the triangles and circle also matches the color of the corresponding experiments.
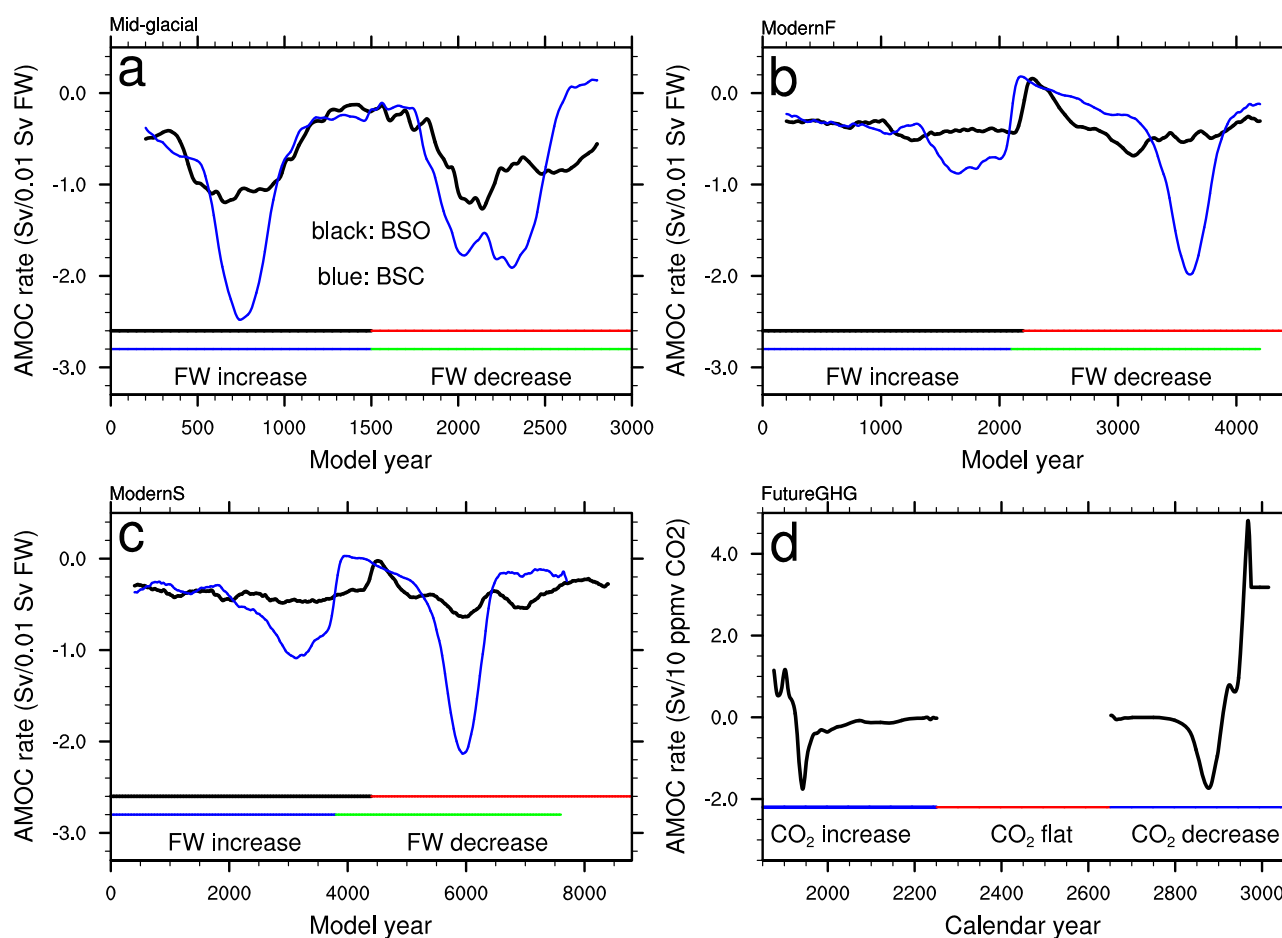
Fig. 2 Running piecewise AMOC change rate. For (**a**–**c**), the AMOC change rate is based on the change in the freshwater flux by 0.01 Sv (Sv(0.01 Sv)$^{-1}$) and black/blue lines represent the open/closed Bering Strait simulations. The straight lines in these three panels show the freshwater increase phase (black/blue) and freshwater decreasing phase (red/green), and open Bering Strait condition (black/red) and closed Bering Strait condition (blue/green). For (**d**), the AMOC change rate is based on the change in CO_2 by 10 ppmv (Sv(10 ppmv)$^{-1}$). The straight lines in this panel represent CO_2 increasing phase (first blue line), CO_2 stabilization phase (red line) and CO_2 decreasing phase (second blue line). The window for piecewise AMOC change rate is 0.008 Sv for (**a**–**c**), and CO_2 changes in 50 calendar years for (**d**). Note that the CO_2 changes are not linear (see Supplementary Fig. 1d). FW represents freshwater. "ppmv" represents parts per million by volume, a unit for CO_2. Note: in freshwater increasing/decreasing phase, a negative trend means increasing/ decreasing freshwater forcing related to a weakening/strengthening of the AMOC. Similarly, a negative trend between AMOC and CO_2 changes means rising/lowering CO_2 related to a weakening/strengthening of the AMOC.
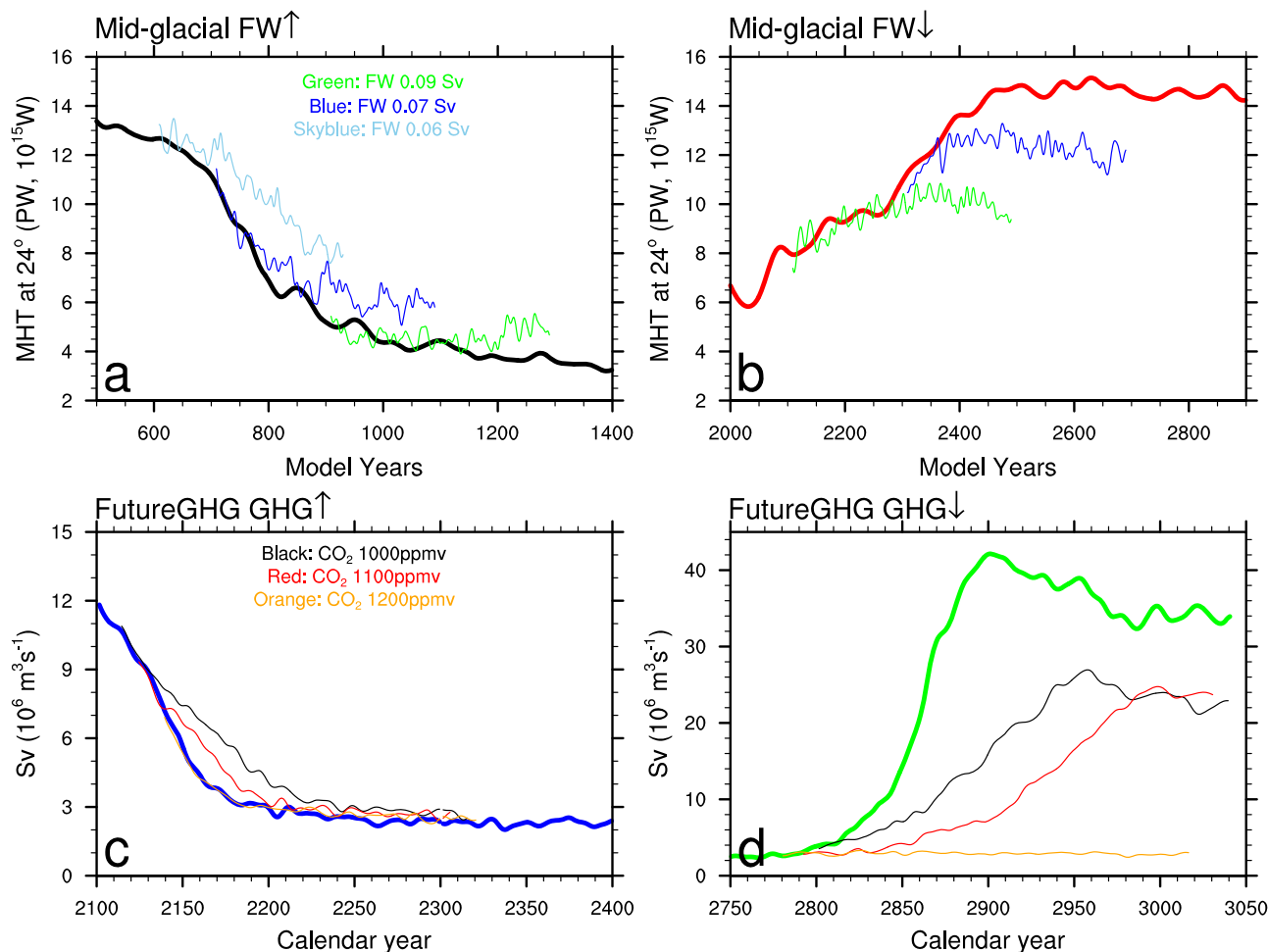
Fig. 3 Changes of AMOC in the sensitivity simulations branched from Mid-glacial-bsc and FutureGHG simulations. (**a**, **b**) show AMOC time series in simulations of Mid-glacial-bsc (black and red lines), freshwater stabilized at 0.07 Sv (blue lines), 0.09 Sv (green lines), and 0.06 Sv (sky blue line) for freshwater increasing (**a**) and decreasing (**b**) phases. (**c**, **d**) show AMOC time series in simulations of FutureGHG (blue and green lines), GHG stabilized at 1000 ppmv (black lines), 1100 ppmv (red lines) and 1200 ppmv (orange lines) during GHG increasing (**c**) and decreasing (**d**) phases. A 13-year Lanczos filter is applied to all data except Mid-glacial-bsc for which a 51-year Lanczos filter is applied.

after the CO_2 concentration stabilizes (2250-2800AD) and including 150 years after the CO_2 concentration starts to decrease (CO_2 changes from 1962 to 1000 ppmv during 2650-2800AD) in the FutureGHG experiment. To further test the AMOC hysteresis under GHG forcing, six sensitivity simulations are branched from this FutureGHG simulation with CO_2 stabilized at 1000, 1100, and 1200 ppmv either before AMOC collapses or before AMOC starts to recover (Fig. 3c, d, and Supplementary Fig. 4b; also see Method section and Table 1 for more details). These simulations show that for the former condition, AMOC collapses with all three stabilization levels (blue triangles in Fig. 1d), with a slower collapsing rate for a lower stabilized CO_2 level. For the latter condition, the AMOC would not recover with CO_2 stabilized at the 1200 ppmv level but recovers with lower stabilized CO_2 levels (green circles in Fig. 1d). The rate of AMOC recovery is smaller with higher stabilized CO_2 level. Thus, we conclude that when the CO_2 level is above 1200 ppmv, AMOC collapses and stays in a collapsed state; when the CO_2 level is higher than 1000 ppmv and lower than 1200 ppmv, the AMOC has two quasi-equilibrium states (blue triangles vs. green circles in Fig. 1d). This further suggests that the AMOC off-state is stable in the FutureGHG experiment since CO_2 stabilizes at a much higher level. Note that this AMOC hysteresis under GHG forcing is also atypical and is

further discussed later. For the processes affect the AMOC collapse and recovery, see Supplementary Note 3.

Therefore, AMOC hysteresis under modern geometry depends on the type of external forcing. While freshwater forcing leads to an absence of hysteresis, GHG forcing results in a clear hysteresis. This difference is associated to the Bering Strait. The open Bering Strait acts as negative feedback for the freshwater-only forced AMOC changes[10,25]. A stronger AMOC pulls additional fresher North Pacific water into the subpolar North Atlantic via the Arctic, and thereby weakening the AMOC, vice versa for a weaker AMOC (Supplementary Figs. 5, 6)[10]. This process prevents the AMOC from collapsing suddenly due to freshwater forcing alone[10]. For FutureGHG, although the volume transport through the Bering Strait declines as AMOC weakens, it shows signs of hysteresis between CO_2 concentrations of 700-1500 ppmv, instead of the linear response experienced by freshwater-forced open Bering Strait simulations. Moreover, freshwater transport across the Bering Strait in FutureGHG is in fact above the control mean throughout the entire simulation, e.g., this freshwater transport increases by approximately 50% when CO_2 concentration rises from 300 to 900 ppmv, contributing to the accelerated collapse of AMOC (Supplementary Figs. 3, 5). This above control run level freshwater transport at Bering Strait also helps maintain

a stable off-state of AMOC in addition to the surface warming. Therefore, this changed role of the Bering Strait freshwater transport under the GHG forcing alone is one of the major factors for the existence of AMOC hysteresis under modern geometry (for more details, see Supplementary Note 3).

Atypical AMOC hysteresis. As mentioned earlier, the AMOC hysteresis for Mid-glacial-bsc and FutureGHG is possibly not typical. For example, in Mid-glacial-bsc, the reactivate loop of the AMOC (red line in Fig. 1a) goes above the AMOC collapse loop (black line in Fig. 1a) when freshwater forcing is below 0.105 Sv (around year 1950 in Supplementary Fig. 2a). For the sensitivity experiments branched from FutureGHG experiment, the final states of the AMOC are weaker in the simulations branched before AMOC collapses than in those simulations branched before AMOC starts to recover. In the other word, when the external forcing (freshwater or GHGs) is stabilized before AMOC collapses, AMOC continuously weakens; when the external forcing is stabilized before or after AMOC starts to recover, AMOC either fully recovers (GHG cases) or strengthens a bit further (freshwater cases). This behavior differs from Figs. 1e-f and the traditional view of the AMOC hysteresis: the reactivate loop of the AMOC should be below the collapse loop of the AMOC in order to show the multi-equilibrium states of the AMOC under the same forcing. Therefore, we may call this as atypical AMOC hysteresis or AMOC anti-hysteresis.

To explore the underlying physical processes causing this behavior in Mid-glacial-bsc, the changes of AMOC and the associated changes in the subpolar North Atlantic are analyzed for model years from 1800 to 2100 with freshwater forcing changing from 0.12 Sv to 0.09 Sv. As shown in Fig. 4, the rising of AMOC by about 3 Sv during years 1935–1955 is associated to an increase of the surface water density in the subpolar region induced by the increase of the surface salinity. The salinity increase is due to the deepened mixed layer that entrains more salty water from the deeper ocean into the upper ocean. Before the deepening of the mixed layer, as the freshwater forcing reduces, the surface temperature in the subpolar region does not change much, but the total sea ice volume and coverage increases, leading to enhanced brine rejection during years 1890–1920. As a result, it destabilizes the stratification and leads to mixed layer deepening and the enhancement of the AMOC. Once AMOC enhances, it leads to an enhanced meridional heat and freshwater convergence in the subpolar North Atlantic[10], resulting in a melt of sea ice and a more stratified ocean, then a shallower mixed layer and a weaker AMOC. Afterward, sea ice formation enhances, more brine rejection which leads to another round of AMOC enhancement. In fact, these processes occurred multiple times in this period with an AMOC enhancement of 2–3 Sv each time, resulting in the activation loop of the AMOC goes above the AMOC collapse loop. The effect of this sea ice related process on AMOC recovery under modern conditions is not as effective as under mid-glacial conditions since the sea ice coverage in the subpolar North Atlantic under modern conditions is much less extensive than under mid-glacial condition. Nevertheless, the recovery of the AMOC under glacial condition may be different from that under modern conditions.

To explain the changes of AMOC in the sensitivity experiments branched from the Mid-glacial-bsc and FutureGHG experiments, we analyzed the water density contrast between surface water and water at 1000 m depth in the subpolar North Atlantic (Fig. 5). For the simulations branched from the forcing increasing phase, the density contrast continues to increase for all cases (Fig. 5), except MGbsc_900 case (see Table 1, green line in Fig. 5a before model year 1500). It is this increased density contrast which leads to the

further weakening or collapsing of the AMOC. For MGbsc_900, the density contrast is nearly unchanged or slightly increases, correspondingly AMOC is also nearly unchanged (green line in Fig. 3a). At the external forcing decreasing phase, AMOC in the simulations branched from Mid-glacial-bsc started to recover already (Fig. 3b). When the freshwater forcing stabilized, the density contrast reduces further in the first 20 to 50 years, then becomes stabilized, so as the AMOC changes. However, for the simulations branched from FutureGHG experiment, AMOC does not start to recover yet (Fig. 3d). When CO_2 concentration is stabilized at different levels, the density contrast slightly increases for GHG_1200d, but decreases a lot for GHG_1000d and GHG_1100d (see Table 1 for the name convention of these experiments), which are consistent with the changes of AMOC in these experiments. The above analysis suggests that the changes of the density contrast between surface water and the water at 1000 m depth basically represent the changes of deep convection in the subpolar North Atlantic and the changes in AMOC strength.

Next, we will explore why the density contrast continues to increase or decrease in these sensitivity experiments. For MGbsc_600 and MGbsc_700 simulations, AMOC is in the process towards collapsing. As the freshwater forcing is stabilized, the freshwater convergence continues to increase in association with the increased freshwater export from the Arctic into the subpolar North Atlantic as indicated by a previous study[10]. As freshwater forcing increases, part of the freshwater added into the subpolar North Atlantic is transported into the Arctic. When the freshwater cumulation in the Arctic reaches a point that no more freshwater can be transported into the Arctic, the freshwater previously transported into the Arctic starts to be transported out of the Arctic, leading to an increased freshwater convergence in the subpolar North Atlantic and a rapid collapse of the AMOC[10]. This can be clearly seen in Supplementary Figs. 7a-r and 8a–i, such that with a linear change in freshwater flux, the surface salinity changes in the closed Bering Strait simulations are not linear. This rapid decrease in surface water salinity leads to the rapid collapse of the AMOC in these closed Bering Strait simulations. On the other hand, for the simulations of MGbsc_2100 and MDbsc_2300, although the freshwater forcing is stabilized, the divergence of the freshwater from the subpolar North Atlantic continues to increase a little bit due the recovery of the AMOC, resulting in a surface salinity slightly higher than that at the beginning of these two runs, thus a slightly further strengthened AMOC.

For GHG_1000u and GHG_1100u, when the CO_2 forcing is stabilized, the surface warming continues since the surface climate has not reached a quasi-equilibrate state with the CO_2 forcing, leading to a further strengthening of the upper ocean stratification in the subpolar North Atlantic, thus a further weakening of the AMOC. For GHG_1000d and GHG_1100d, the global mean climate is on the decreasing trend as CO_2 has been declining from the peak (1962 ppmv). At the same time, the subsurface water, such as water at 1000 m depth, becomes much warmer (as it has experienced the peak level of CO_2 for 400 years; Supplementary Fig. 7s–u) than that during CO_2 increasing phase. This cooling for the surface water and warming for the subsurface water reduces the density contrast between surface and subsurface waters, and weakens the vertical stratification of the water column, leading to a strengthening of the deep convection and a recovery of the AMOC.

From Fig. 5b–d, one can see that for ModernF_bsc, ModernS_bsc and FutureGHG experiments, AMOC collapses after the density contrast is greater than $2.5–3 \, kg \, m^{-3}$, and AMOC recovers if this density contrast is smaller than $2.5–3 \, kg \, m^{-3}$. The density contrast for Mid-glacial_bsc is a bit
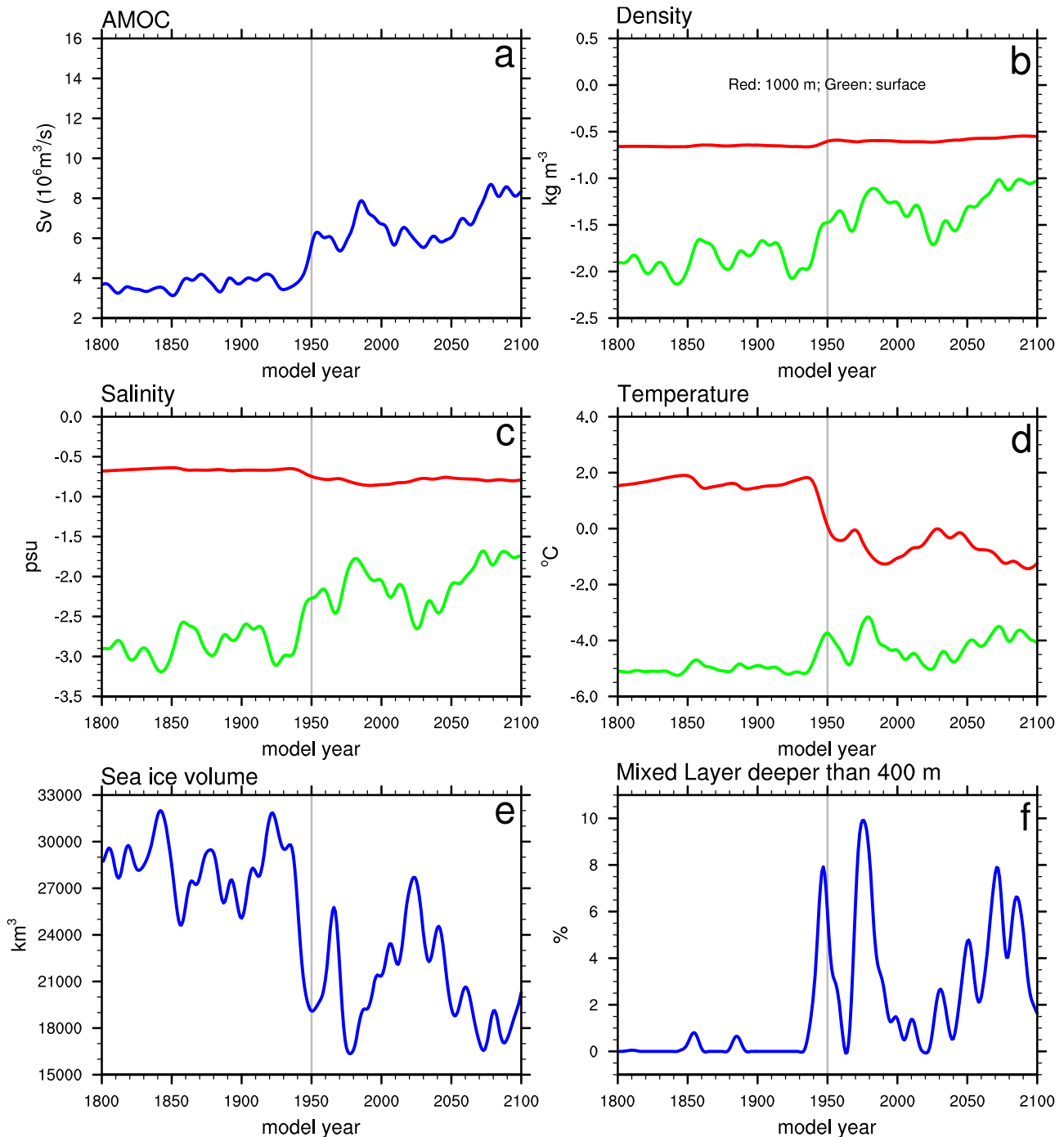
Fig. 4 AMOC, density, salinity, temperature, sea ice volume and mixed layer depth in the subpolar North Atlantic during model years 1800–2100 in Mid-glacial-bsc. Panel **a** is AMOC time series. For density (**b**), salinity (**c**), and temperature (**d**), green lines are for surface and red lines for 1000 m depth. Panel **e** is sea ice volume. For mixed layer (**f**), it is the percentage of the March mixed layer depth deeper than 400 m over the total area in the subpolar North Atlantic.

higher (~3.8 kg m^{-3}, Fig. 5a). This may suggest that once a critical point for the density contrast is crossed, a collapse/reactivate of the AMOC becomes unavoidable.
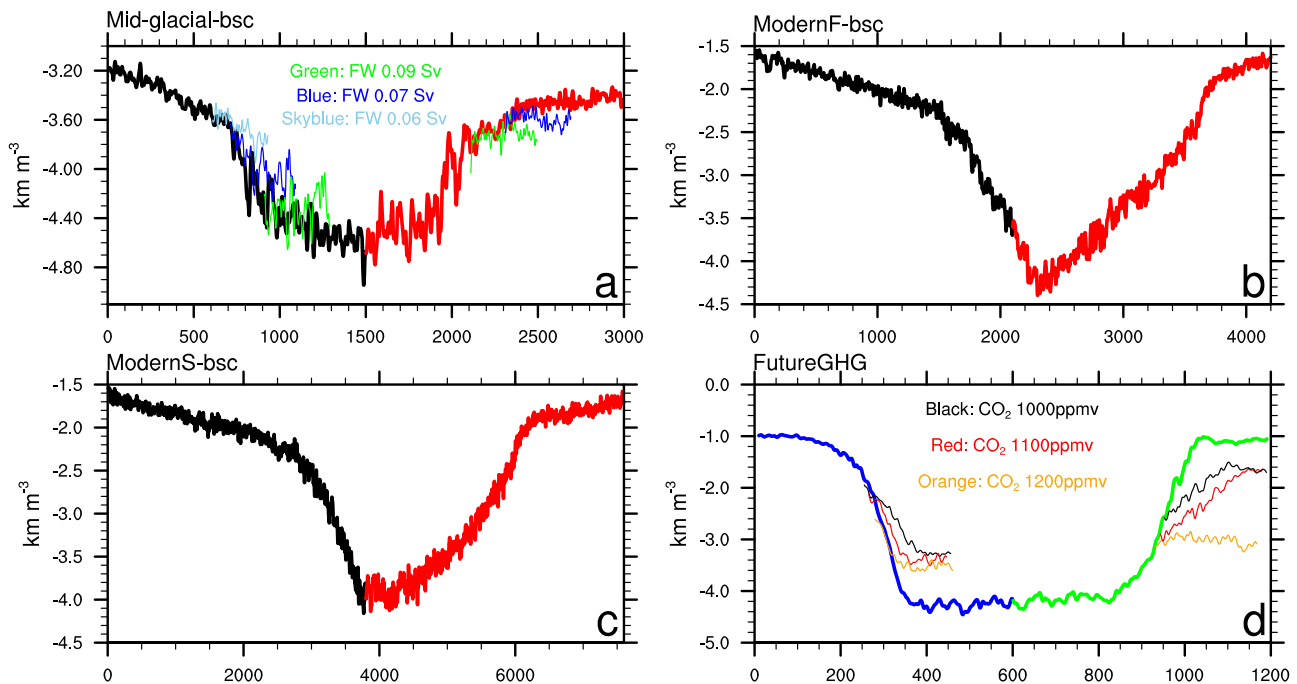
Influence of AMOC on global and regional surface climate. Since AMOC is an important part of the global energy balance, large changes in AMOC affect the surface climate in not only the subpolar North Atlantic, but also globally[19,25,26]. As AMOC progresses from a weakened to a collapsed state in response to changes in freshwater forcing, global mean temperature decreases

by a maximum of ~1 °C under Modern conditions and ~1.5 °C under Mid-glacial conditions (Supplementary Fig. 9a-f, red lines). Hemispherically, there is larger cooling (up to 2.5–3°C) in the Northern Hemisphere, but a slight warming (up to 0.5 °C) or a much weaker cooling in the Southern Hemisphere (Supplementary Table 1 and Supplementary Figs. 9–12) in association with the reduced oceanic meridional heat transport (Supplementary Figs 13a-c). Latitudinally, the cooling is mainly in the mid-high northern latitudes and the warming in the southern mid-latitudes (Supplementary Figs. 10a-f and 12a-f). With GHG forcing alone,

Fig. 5 Density difference between the water at surface and 1000 m depth in the subpolar North Atlantic. Black/red lines are for the closed Bering Strait simulations as freshwater forcing increases/decreases (**a–c**). Blue/green line is for the FutureGHG experiment as CO_2 increases/decreases (**d**). Other color lines shown in (**a, d**) are explained within each of the panels, and the color convention in these two panels are the same as in Fig. 3.

the warming is initially faster and higher in the Northern than the Southern Hemisphere due primarily to the amplified polar warming and the faster warming over land (Supplementary Figs. 9g, 10g, 11g, 12g–h). However, after AMOC collapses, the temperature rises more in the Southern than the Northern Hemisphere in association with a reduced northward meridional oceanic heat transport (Supplementary Figs. 13d). The amplified warming in the southern polar region (Supplementary Figs. 9–12) is due to the disappearance of sea ice and snow melt on ice sheet surface that lowers the surface albedo and allows more sunlight to be absorbed.

Figures 6–8 show the time evolution of the global and hemispheric precipitation, evaporation and cloudiness in these experiments. In response to a weakened to collapsed AMOC under freshwater forcing, there are reductions of precipitation, evaporation, and cloudiness in the Northern Hemisphere and increases in the Southern Hemisphere with a net reduction globally for precipitation and evaporation, but an increase globally for cloudiness (Figs. 6a–f, 7a–f, and 8a–f). Vice versa for the AMOC strengthening phase. These changes are smaller in simulations with a closed Bering Strait than in simulations with an open Bering Strait regardless the background climate states. The smaller changes of these climate properties in the closed Bering Strait simulations are related to the setup of the Pacific deep overturning circulation which increases the northward meridional heat transport in the Pacific basin, partially compensated the northward meridional heat transport reduction in the Atlantic basin[40]. Further decompositions show that the largest reduction in precipitation and evaporation is in the northern Polar Regions, and the reduction in precipitations is obvious in northern mid-low latitudes, but only mid-latitudes for evaporation (Supplementary Figs. 14a–f, 15a–f; Supplementary Tables 2 and 3). The increased precipitation is mainly in the southern low-latitudes in association with the southward movement of inter-tropical convergence zone (ITCZ)[41–43], and the increased

evaporation is in the southern mid-low latitudes in association to the warming induced by the collapsed AMOC. The decreased cloudiness in the Northern Hemisphere is located mainly in the low and high-latitudes with an increase in the mid-latitudes, and the increase of the cloudiness in the Southern Hemisphere occurs mostly in the southern low-latitudes with smaller decrease in the southern mid-high latitudes (Supplementary Fig. 16a–f). Therefore, we can conclude that qualitatively, the influence of a collapsed AMOC due to freshwater forcing on precipitation, evaporation and cloudiness is independent from the background climate condition and the status of the Bering Strait; quantitatively, this influence is larger with an open Bering Strait than a closed Bering Strait regardless the background climate.

For FutureGHG simulation, there are increased precipitation, evaporation and cloudiness on global and hemispheric scales due to the GHG induced intensification of the hydrological cycle. However, these changes for precipitation and evaporation are smaller in the Northern Hemisphere than those changes in Southern Hemisphere. The difference of precipitation and evaporation changes between two Hemispheres with a collapsed AMOC in FutureGHG is roughly the same as those in the ModernS_bso and ModernF_bso (~0.5 mm day^{-1} for precipitation and ~0.2 mm day^{-1} for evaporation, Figs. 6g–7g; Supplementary Tables 2 and 3). This result suggests that the different changes in precipitation and evaporation between two Hemispheres are mostly due to the collapsed AMOC. Further decomposition also indicates that for evaporation, the largest contribution to the increase in Southern Hemisphere is the southern mid-latitudes, and the largest contribution to the decrease is the northern mid to high-latitudes, consistent with the results forced by freshwater only (Supplementary Fig. 15). For precipitation, the more increase in the Southern Hemisphere than the global mean is mainly contributed from southern polar region with minor contribution from southern low-latitudes, and the less than global mean increase in the Northern Hemisphere is mainly
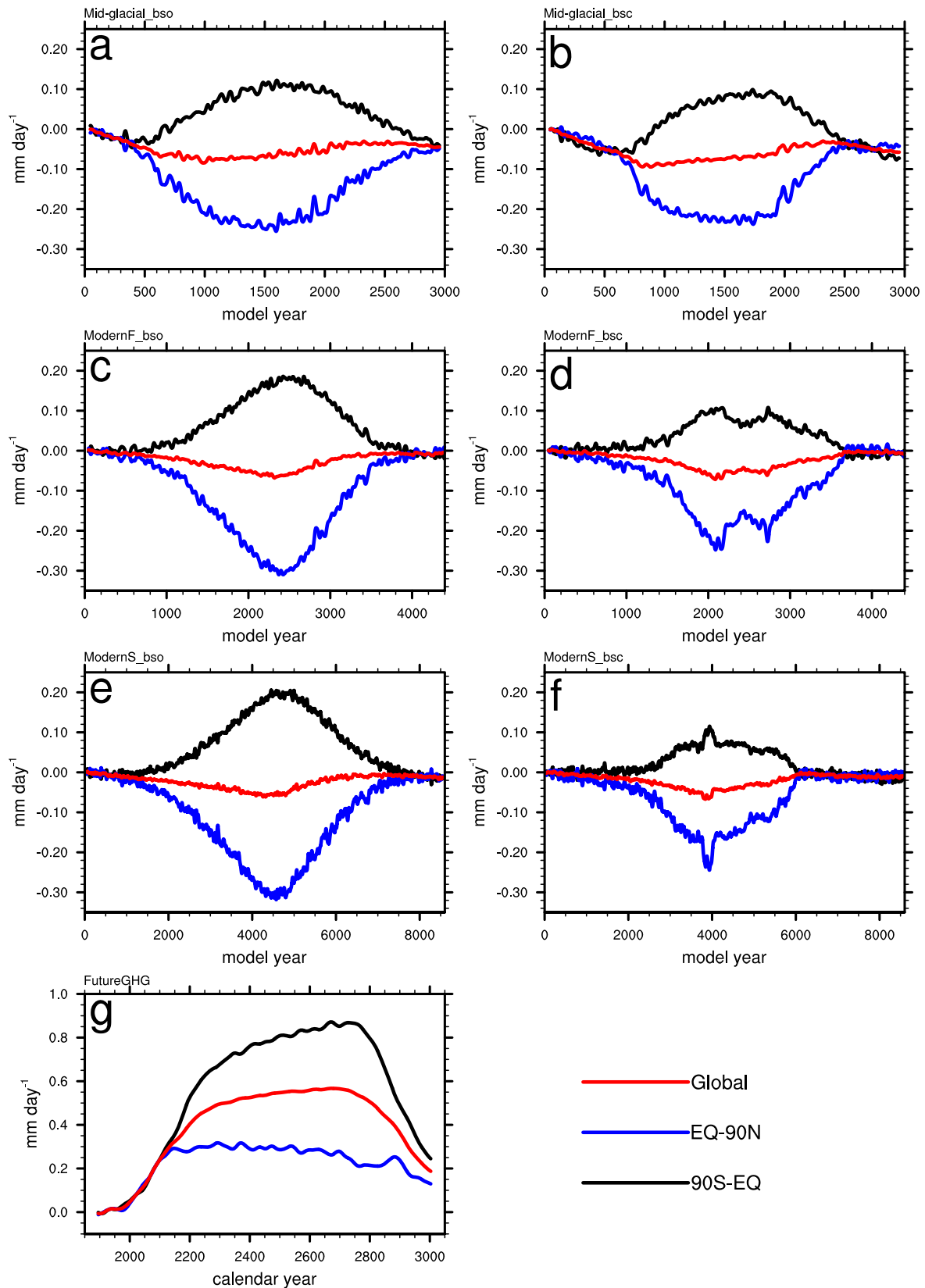
Fig. 6 Changes of annual mean precipitation. bso/bsc represent simulations with open/closed Bering Strait (**a**–**f**). Global/EQ-90N/90S-EQ (red/blue/black lines) represents global/Northern Hemispheric/Southern Hemispheric mean (**a**–**g**). ModernF/ModernS is for modern climate background with faster/slower freshwater flux increment per year (**c**–**f**); Mid-glacial is for mid-glacial background climate (15 ka BP; **a**, **b**); FutureGHG is for future climate condition (**g**).
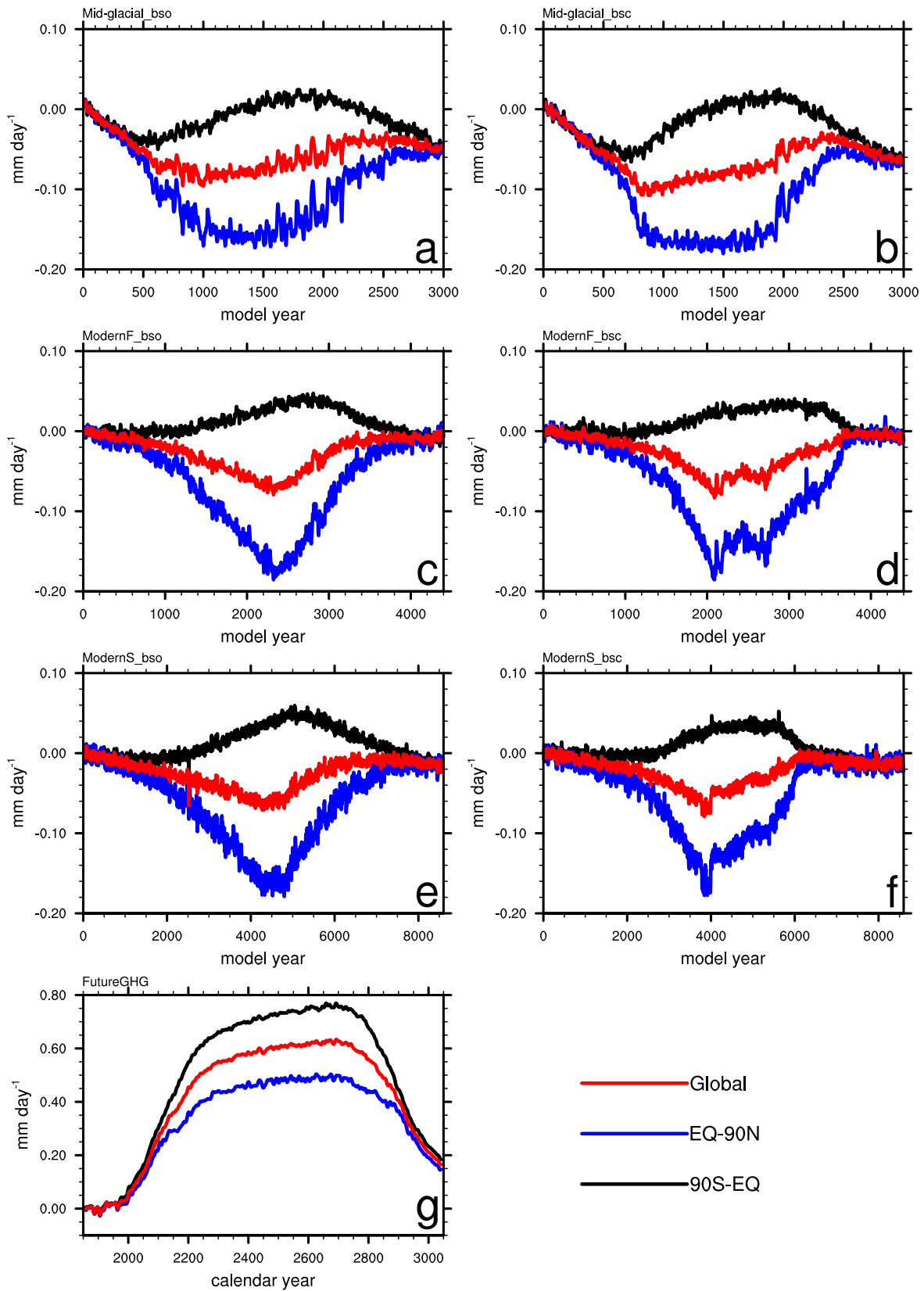
Fig. 7 Changes of annual mean evaporation. bso/bsc represent simulations with open/closed Bering Strait (**a–f**). Global/EQ-90N/90S-EQ (red/blue/black lines) represents global/Northern Hemispheric/Southern Hemispheric mean (**a–g**). ModernF/ModernS is for modern climate background with faster/slower freshwater flux increment per year (**c–f**); Mid-glacial is for mid-glacial background climate (15 ka BP; **a–b**); FutureGHG is for future climate condition (**g**).
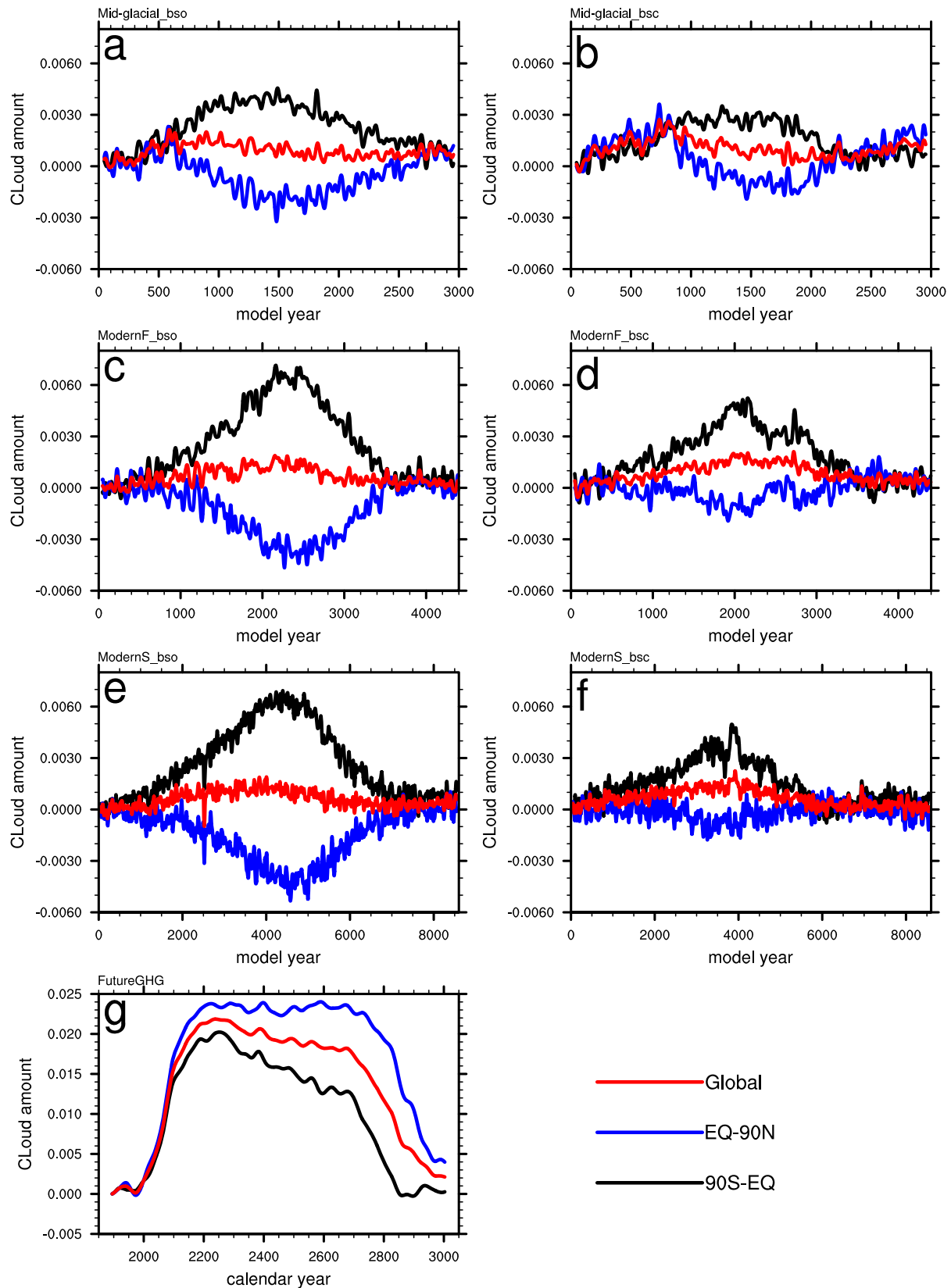
Fig. 8 Changes of annual mean total cloud cover. bso/bsc represent simulations with open/closed Bering Strait (**a–f**). Global/EQ-90N/90S-EQ (red/blue/black lines) represents global/Northern Hemispheric/Southern Hemispheric mean (**a–g**). ModernF/ModernS is for modern climate background with faster/slower freshwater flux increment per year (**c–f**); Mid-glacial is for mid-glacial background climate (15 ka BP; **a**, **b**); FutureGHG is for future climate condition (**g**).

contributed from northern low-latitudes with some contribution from northern mid-latitudes (Supplementary Fig. 14). The larger precipitation change in both Polar Regions is associated to the polar amplified warming[44]. Therefore, due to the collapsed AMOC, the precipitation changes in different latitude bands relative to the global mean are also in agreement with those changes in the freshwater forced experiments except the Polar Regions.

For cloudiness, the increase is larger for the Northern than the Southern Hemisphere. This difference is mainly due to the larger increase in cloudiness in the northern polar region than that in the southern polar region (Fig. 8g and Supplementary Fig. 16g). In addition, there is nearly no change for cloudiness in the northern low to mid-latitudes, but the cloudiness changes in southern low- and mid-latitudes are opposite to each other with an increase for the former but a decrease for the latter (Supplementary Fig. 16g and Supplementary Table 4). Moreover, the area-weighted increase of cloudiness in the low latitudes is less than the area-weighted decrease in mid-latitudes. This in combination with the less cloud increase in the southern polar region leads to a less cloud increase in the Southern Hemisphere than that in the Northern Hemisphere. Thus, in response to GHG forcing, the cloudiness increased largely in both Polar Regions in relation to the polar amplified warming. Except these two regions, the changes in cloudiness in FutureGHG experiment, in fact, agree with the freshwater forced experiment in the southern low to mid-latitudes with nearly muted changes in the northern low to mid-latitudes. Therefore, the GHG forcing does modulate the response of the cloudiness to the collapse of the AMOC on both regional and global scale.

Discussion

In summary, the existence of AMOC hysteresis due to freshwater forcing alone does not depend on the background mean climate but rather on the status of the Bering Strait. AMOC hysteresis exists with a closed Bering Strait (true for glacial conditions), but is absent when the Bering Strait is open (true for modern conditions), because throughflow across the Bering Strait plays a negative feedback role that prevents the AMOC from collapsing suddenly. However, with GHG forcing alone under modern geographic conditions, AMOC hysteresis can exist since the GHG forcing has modulated the negative feedback role for Bering Strait throughflow via changes in the hydrological cycle. Although the total volume transport across the Bering Strait is reduced as AMOC weakens in FutureGHG simulation, the freshwater transport via this strait from the Pacific into the subpolar North Atlantic increases as the subpolar North Pacific freshens due to increased precipitation. Because this fresher upper ocean due to the increased freshwater transport via Bering Strait is compounded by the GHG induced surface warming, the upper ocean stratification in the subpolar North Atlantic becomes much stronger, inducing a rapid collapse of AMOC. Our results further suggest that with a collapsed AMOC, the surface temperature, precipitation, evaporation and cloudiness decrease in Northern Hemisphere, but increase in Southern Hemisphere. Under GHG forcing alone, the changes of these variables generally agree with those under freshwater forcing alone, and the differences show up mainly in the Polar Regions in association to the feedbacks due to the amplified warming there.

It is worth pointing out that AMOC in the freshwater-forced simulations is in a quasi-equilibrium (or equilibrium) state with the external forcing changes since the rate of freshwater forcing change is small. However, the GHG changes in our FutureGHG experiment are so rapid that it is almost impossible for the changes in AMOC and the GHG forcing to be in a quasi-equilibrium state during AMOC decline/recovery phases. In general, our results under freshwater forcing agree with many previous studies on AMOC hysteresis using simpler models with a closed Bering Strait[11,12,30,32]. For the GHG forcing, one study using a low-resolution coupled model under glacial conditions suggests that a slow increase in CO_2 concentration is capable of changing AMOC from a weak stadial state to a strong interstadial state due primarily to changes in surface salinity[45]. Another study using a low-resolution coupled model showed that a rapid rise in CO_2 resulted in a weakening of AMOC; hundreds of simulated years at a higher CO_2 concentration will eventually result in a strengthening of AMOC[46] which is consistent with the results under glacial conditions[45]. In other words, the equilibrium response of AMOC to elevated CO_2 forcing could be a strengthening of AMOC due to either elevated surface salinity[45] or weakened vertical stratification in association with the warming of subsurface water layers[46]. Note that due to the coarse ocean resolution, the Bering Strait is closed in these two models, which may induce a response of AMOC to GHG forcing differs from that in our FutureGHG experiment. Finally, the similarity of the differences between precipitation (or evaporation or surface temperature) changes in the Northern and Southern Hemispheres in the freshwater forced or GHG forced experiments are strong evidence to indicate that if the same version of the CCSM model is used for all our simulations, the same conclusion will be reached. In addition, while the details of AMOC response to GHG or freshwater forcing could be model dependent, the general conclusions reached here should be model independent.

Method

Models. The coupled models used in this study are the Community Climate System Model versions 3 and 4 (CCSM3 and CCSM4)[28,29]. The horizontal resolution for the ocean and sea ice components in both versions of CCSM is nominal one degree with enhanced meridional resolution to 1/3 degree in the equatorial tropics. The ocean model vertical resolution is 40 levels for CCSM3, but 60 levels for CCSM4. The major changes for the CCSM4 ocean model are the addition of the overflow parameterization in the subpolar North Atlantic along with a few other changes. The horizontal resolution for the atmospheric and land components is T42 (about 2.8 degree) for CCSM3, and one degree for CCSM4. The dynamic core is spectral for CCSM3, but finite volume for CCSM4 with some changes in atmospheric deep convection and cloud physics[29]. Both models are able to simulate the observed 20th-century climate reasonably well[47,48]. The mean AMOC strength in the control run is ~15 Sv for CCSM3 mid-glacial conditions, ~20 Sv for CCSM3 present day conditions and ~25 Sv for CCSM4 preindustrial conditions.

Here we acknowledge that two versions of CCSM model have been used in our study. Previous assessments[47,48] on the AMOC's response to GHG forcing in these two versions of CCSM indicate that the AMOC changes are similar for the comparable future climate scenarios, e.g., IPCC Special Report on Emissions Scenarios (SRES) A1B used in CCSM3 for coupled model intercomparison project phase 3 (CMIP3) vs. Representative Concentration Pathway 6.0 (RCP6.0) used in CCSM4 for CMIP5. The maximum CO_2 concentration is about 9% higher in the latter than the former scenario (see Fig. 1 in ref. [48] for the changes in GHGs, and Fig. 4c in ref. [47] and Fig. 15 in ref. [48] for AMOC changes). The mean state of AMOC in the preindustrial control run is 22 Sv for CCSM3 and 25 Sv for CCSM4 and the maximum decline of the AMOC is ~5 Sv for CCSM3 and ~6 Sv for CCSM4 (CCSM3 SRES A1B scenario and CCSM4 RCP6.0 scenario)[47,48]. In addition, the influence of Bering Strait status on the AMOC mean state is also similar in these two versions of CCSM, such as AMOC is stronger with a closed Bering Strait than that with an open Bering Strait[49,50]. Thus, if the same version of CCSM were used for all experiments discussed here, we expect that qualitatively similar results will be obtained. For AMOC's response to various GHG forcing in CCSM3 and CCSM4, see Supplementary Note 4.

Experiments. For mid-glacial or 15 thousand years before present (BP) conditions (Mid-glacial or 15 ka BP), CO_2 concentration is set to 214 ppmv and methane (CH_4) is at 350 parts per billion by volume (ppbv)[21,49,51]. The surface vegetation, Laurentide Ice Sheet[52] and orbital forcing are all at 15 ka level. Under this condition, one set of paired simulations are carried out in which one simulation is run with an open Bering Strait (bso, hypothetical) and the other with a closed Bering Strait (bsc) using CCSM3 (referenced as Mid-glacial_bso and Mid-glacial_bsc; Supplementary Fig. 1a). Here, the closed Bering Strait condition is the true condition for Mid-glacial. The open Bering Strait experiment is a hypothetical construct that we use to evaluate the impact of flow through the Bering Strait on the

stability of AMOC under glacial conditions. As suggested earlier[6,10], the Bering Strait may have opened or closed more than once during the last glaciation and may have influenced the stability of AMOC and, consequently, global climate. The added freshwater flux is uniformly distributed into the North Atlantic between 50 and 70ºN. The initial amount of added freshwater flux is 0.0001 Sv (1 Sv ≡ $10^6 m^3$ s^{-1}) or 100 m^3 s^{-1} with an annual increment of the same amount (0.0001 Sv $year^{-1}$ or 100 m^3 $s^{-1}year^{-1}$), such that the increase from 0.0 to 0.1 Sv will take 1000 years. Once the AMOC collapses, the added freshwater flux is decreased linearly by the same amount until AMOC reactivates. Both simulations are run for 3000 model years with the freshwater forcing ramping up for 1500 years and ramping down for another 1500 years. The initial control simulation with an open Bering Strait is branched from a 112 ka BP simulation (with CO_2 fixed at 257 ppmv and CH_4 at 456 ppbv)[49,51,53] and is run for 1100 years. The closed Bering Strait control run is branched from the open Bering Strait control at year 200 and is run for 900 years. The freshwater forced simulations are branched from the open Bering Strait control at year 400 (Mid-glacial_bso) and from the closed Bering Strait control run at year 200 (Mid-glacial_bsc).

Additional sensitivity simulations are carried out to test the AMOC stability under mid-glacial condition with a closed Bering Strait. These simulations are branched from Mid-glacial_bsc at years 600, 700, 900, 2100, and 2300. For the starting years of 600, 700, and 900, the AMOC is rapidly weakening, but not collapsed yet (Fig. 1a and Supplementary Fig. 2a). For the starting years of 2100 and 2300, AMOC is rapidly recovering, but not fully recovers yet. All these simulations were run for 400 years except the one that branched at year 600 and was run for 340 years. The freshwater forcing is stabilized at 0.06 Sv for the experiment that branched at year 600; 0.07 Sv for the ones that branched at years 700 and 2300; and 0.09 Sv for the ones that branched at years 900 and 2100. These experiments are referenced as MGbsc_600, MGbsc_700, MGbsc_900, MGbsc_2100, MGbsc_2300 (see Table 1). Therefore, MGbsc_700 and MGbsc_2300 are paired experiments with the same stabilized freshwater forcing level (0.07 Sv) but are branched from the freshwater increasing and decreasing phases, respectively. It is the same for MGbsc_900 and MGbsc_2100.

Under modern (1990AD) conditions (Modern), two sets of paired simulations are carried out with additional freshwater flux added uniformly into the North Atlantic between 20 and 50ºN using CCSM3 to avoid the direct impact of this added freshwater on the deep convection in the subpolar North Atlantic as suggested by previous work[11,12]. Within each set, one simulation is run with an open Bering Strait (bso; the real world experiment) and the other with a closed Bering Strait (bsc; the hypothetical experiment). The initial amount of added freshwater flux for the first pair is 200 m^3 s^{-1} (0.0002 Sv), and 100 m^3 s^{-1} (0.0001 Sv) for the second pair. The annual increment of freshwater forcing is the same as the initial amount in both pairs until the AMOC collapses (Supplementary Fig. 1b, c). These conditions are named: "modern climate, fast freshwater increment" (ModernF) for the former and "modern climate, slow freshwater increment" (ModernS) for the latter, respectively. After AMOC collapses, we reduce the freshwater flux by 0.0002 or 0.0001 Sv per year until the AMOC reactivates. This represents a way to test the AMOC hysteresis loop as proposed by a previous study[30]. With a freshwater changing rate of 0.0002 Sv, the model simulations run about 4500 model years, and with a freshwater flux changing rate of 0.0001 Sv, the model simulations run about 9000 model years. All these experiments are branched from the same year from a 1990 control simulation with all forcings kept constant at 1990AD (e.g., CO_2 concentration at 355 ppmv). Note that the duration difference between modern (~9000 model years) and mid-glacial (~3000 model years) conditions at a freshwater flux rate of 100 m^3 $s^{-1}year^{-1}$ increment is because the additional freshwater is added into the subtropical North Atlantic (indirectly affecting the AMOC-related deep convection) for the modern condition, but subpolar North Atlantic (directly affecting the AMOC-related deep convection) for the mid-glacial condition. The purpose of these two sets of paired experiments is to test whether the rate of the added freshwater flux would affect the AMOC hysteresis behavior. These experiments are referenced as ModernF_bso, ModernF_bsc, ModernS_bso, and ModernS_bsc.

For future climate, the simulation is branched from the CCSM4 preindustrial control simulation and run under 20th-century historical forcing from 1850 to 2005AD. The future period (2006-2300AD) is run under representative concentration pathway 8.5 (RCP8.5) forcing. From 2301-2600AD, all forcings are kept at RCP8.5 2300 level in order to allow the AMOC and surface climate to reach a quasi-equilibrium state with the external forcings (Supplementary Fig. 1d)[31]. Afterwards, the RCP8.5 forcing is reversed to ramp down to 2005 levels over years 2601–2895AD and down to 1850 levels over years 2896–3050AD. For this experiment, the Bering Strait is open and the primary change in forcing comes from GHG concentrations: CO_2 changes from 285 ppmv at 1850AD to 1962 ppmv at 2250AD (Supplementary Fig. 1d). Therefore, this experiment is used to test the changes of GHG forcing on AMOC hysteresis and is referenced as FutureGHG. The total length of this experiment is 1200 years.

To test the stability of AMOC under different stabilized GHG levels, we branched 6 simulations from the FutureGHG run with GHG stabilized at 1000, 1100, and 1200 ppmv during GHG increase phase (3 simulations; before AMOC collapses) and GHG decreasing phase (3 simulations; before AMOC starts to recover). These simulations are run for 200 or more years each and branched from FutureGHG at calendar years 2105 (~1000 ppmv), 2115 (~1100 ppmv), 2130 (~1200 ppmv), 2771 (~1200ppmv), 2783 (~1100 ppmv), and 2792 (~1000 ppmv).

They are referenced as GHG_1000u, GHG_1100u, and GHG_1200u (u, up) for CO_2 rising phase, and GHG_1000d, GHG_1100d, and GHG_1200d (d, down) for CO_2 decreasing phase (Table 1). In the other word, we run 3 paired experiments with CO_2 concentration stabilized at three different levels (1000, 1100, 1200 ppmv, respectively). Within each pair, one simulation is branched from FutureGHG experiment in the CO_2 rising phase and the other in the CO_2 decreasing phase.

Data availability
The datasets and NCL scripts used to generate all figures for this publication are available through https://zenodo.org/record/8075707.

Code availability
The models can be found at https://www.earthsystemgrid.org/dataset/ucar.cgd.ccsm.src.3.0.0.0.html for CCSM3 and https://www.cesm.ucar.edu/models/ccsm4.0/ for CCSM4.

References
1. Heinrich, H. Origin and consequences of cyclic ice rafting in the northeast Atlantic Ocean during the past 130,000 years. *Quat. Res.* **29**, 143–152 (1988).
2. Hemming, S. R. Heinrich events: massive late Pleistocene detritus layers of the North Atlantic and their global climate imprint. *Rev. Geophys.* **42**, RG1005 (2004).
3. Lynch-Stieglitz, J. The Atlantic Meridional Overturning Circulation and abrupt climate change. *Annu. Rev. Mar. Sci.* **9**, 83–104 (2017).
4. Dansgaard, W. et al. Evidence for general instability for past climate from a 250-kyr ice-core record. *Nature* **364**, 218–220 (1993). (1993).
5. Ditlevsen, P. D., Kristensen, M. S. & Andersen, K. K. The recurrence time of Dansgaard-Oeschger events and limits on the possible periodic component. *J. Clim.* **18**, 2594–2603 (2005).
6. Hu, A. et al. Influence of Bering Strait flow and North Atlantic circulation on glacial sea level changes. *Nat. Geosci.* **3**, 118–121 (2010).
7. North Greenland Ice Core Project members. High-resolution record of Northern Hemisphere climate extending into the last interglacial period. *Nature* **431**, 147–151 (2004).
8. Trenberth, K. & Fasullo, J. Atlantic meridional heat transports computed from balancing Earth's energy locally. *Geophys. Res. Lett.* **44**, 1919–1927 (2017).
9. Dong, S., Garzoli, S., Baringer, M., Meinen, C. & Goni, G. Interannual variations in the Atlantic meridional overturning circulation and its relationship with the net northward heat transport in the South Atlantic. *Geophys. Res. Lett.* **36**, L20606 (2009).
10. Hu, A. et al. Role of the Bering Strait on the hysteresis of the ocean conveyor belt circulation and glacial climate stability. *Proc. Natl Acad. Sci.* **109**, 6421–6422 (2012).
11. Rahmstorf, S. Bifurcations of the Atlantic Thermohaline circulation in response to changes in the hydrological cycle. *Nature* **378**, 145–149 (1995).
12. Ganopolski, A. & Rahmstorf, S. Rapid changes of glacial climate simulated in a coupled climate model. *Nature* **409**, 153–158 (2001).
13. Alley, R. B., Clark, P. U., Keigwin, L. D. & Webb, R. S. Making sense of millennial-scale climate change. *Geophys. Monograph-Am. Geophys. Union* **112**, 385–394 (1999).
14. Boning, C. W., Behrens, E., Biastoch, A., Getzlaff, K. & Bamber, J. L. Emerging impact of Greenland meltwater on deep water formation in the North Atlantic Ocean. *Nat. Geosci.* **9**, 523–527 (2016).
15. Caesar, L., McCarthy, G. D., Thornalley, D. J. R., Cahill, N. & Rahmstorf, S. Current Atlantic Meridional Overturning Circulation weakest in last millennium. *Nat. Geosci.* **14**, 118–120 (2021).
16. Boers, N. Observation-based early-warning signals for a collapse of the Atlantic Meridional Overturning Circulation. *Nat. Clim. Chang.* **11**, 680–688 (2021).
17. Stouffer, R. J. et al. Investigating the causes of the response of the thermohaline circulation to past and future climate changes. *J. Clim.* **19**, 1365–1387 (2006).
18. Hu, A., Meehl, G. A. & Han, W. Role of the Bering Strait in the thermohaline circulation and abrupt climate change. *Geophys. Res. Lett.* **34**, L05704 (2007).
19. Hu, A. et al. Influence of continental ice retreat on future global climate. *J. Clim.* **26**, 3087–3111 (2013).
20. Lambeck, K., Rouby, H., Purcell, A., Sun, Y. & Sambridge, M. Sea level and global ice volumes from the Last Glacial Maximum to the Holocene. *Proc. Natl Acad. Sci.* **111**, 15296–15303 (2014).

21. Deschamps, P. et al. Ice-sheet collapse and sea-level rise at the Bolling warming 14,600 years ago. *Nature* **483**, 559–564 (2012).

22. Gregory, J. M. et al. A model intercomparison of changes in the Atlantic thermohaline circulation in response to increasing atmospheric CO2 concentration. *Geophys. Res. Lett.* **32**, L12703 (2005).

23. Levang, S. J. and Schmitt, R. W. What causes the AMOC to weaken in CMIP5. *J. Clim.* **33**, 1535–1545 (2020).

24. Hu, A., Meehl, G. A., Han, W. & Yin, J. Transient response of the MOC and climate to potential melting of the Greenland Ice Sheet in the 21st century. *Geophys. Res. Lett.* **36**, L10707 (2009).

25. Hu, A., Meehl, G. A., Han, W. & Yin, J. Effect of the potential melting of the Greenland Ice Sheet on the Meridional Overturning Circulation and global climate in the future. *Deep Sea Res. II* **58**, 1914–1926 (2011).

26. Stouffer, R. J., Seidov, D. & Haupt, B. J. Climate response to external sources of freshwater: North Atlantic versus the Southern Ocean. *J. Clim.* **20**, 436–448 (2007).

27. Bakker, P. et al. Fate of the Atlantic Meridional Overturning Circulation: Strong decline under continued warming and Greenland melting. *Geophys. Res. Lett.* **43**, 12,252–12,260 (2017).

28. Collins, W. et al. The Community Climate System Model: CCSM3. *J. Clim.* **19**, 2122–2143 (2006).

29. Gent, P. R. et al. The Community Climate System Model Version 4. *J. Clim.* **24**, 4973–4991 (2011).

30. Rahmstorf, S. et al. Thermohaline circulation hysteresis: a model intercomparison. *Geophys. Res. Lett.* **32**, L23605 (2005).

31. Hu, A., Meehl, G. A., Han, W., Lu, J. & Strand, W. G. Energy balance in a warm world without the ocean conveyor belt and sea ice. *Geophys. Res. Lett.* **40**, 6242–6246 (2013).

32. Stocker, T. F. & Wright, D. G. Rapid transitions of the ocean's deep circulation induced by changes in surface water fluxes. *Nature* **351**, 729–732 (1991).

33. Cheng, W., Chiang, J. C. H. & Zhang, D. Atlantic Meridional Overturning Circulation (AMOC) in CMIP5 Models: RCP and historical simulations. *J. Clim.* **26**, 7187–7197 (2013).

34. Weijer, W., Cheng, W., Garuba, O. A., Hu, A. & Nadiga, B. T. CMIP6 models predict significant 21st century decline of the Atlantic Meridional Overturning Circulation. *Geophys. Res. Lett.* **47**, e2019GL086075 (2020).

35. Hu, A. et al. Role of AMOC in transient climate response to greenhouse gas forcing in two coupled models. *J. Clim.* **33**, 5845–5859 (2020).

36. Hu, A., Meehl, G. A., Washington, W. M. & Dai, A. Response of the Atlantic thermohaline circulation to increased atmospheric CO2 in a coupled model. *J. Clim.* **17**, 4267–4279 (2004).

37. Wu, P., Jackson, L., Pardaens, A. & Schaller, N. Extended warming of the northern high latitudes due to an overshoot of the Atlantic meridional overturning circulation. *Geophys. Res. Lett.* **38**, L24704 (2011).

38. Haskins, R. K., Oliver, K. I. C., Jackson, L. C., Drijfhout, S. S. & Wood, R. A. Explaining asymmetry between weakening and recovery of the AMOC in a coupled climate model. *Clim. Dyn.* **53**, 67–79 (2019).

39. Weijer, W. et al. Stability of the Atlantic Meridional Overturning Circulation: a review and synthesis, *J. Geophys. Res. Ocean* **124**, https://doi.org/10.1029/2019JC015083 (2019).

40. Hu, A. et al. The Pacific-Atlantic Seesaw and the Bering Strait. *Geophys. Res. Lett.* **39**, L03702 (2012).

41. Donohoe, A., Marshall, J., Ferreira, D., & McGee, D. The relationship between ITCZ location and atmospheric heat transport across the equator: from the seasonal cycle to the Last Glacial Maximum. *J Clim.* **26**, 3597–3618 (2013).

42. Donohoe, A., Marshall, J., Ferreira, D., Armour, K., & McGee, D. The interannual variability of tropical precipitation and interhemispheric energy transport. *J Clim.* **27**, 3377–3392 (2014).

43. Liu, W. & Hu, A. The role of the PMOC in modulating the deglacial shift of the ITCZ. *Clim. Dyn.* **45**, 3019–3034 (2015).

44. Bintanja, R. The impact of Arctic warming on increased rainfall. *Sci. Rep.* **8**, 16001 (2018).

45. Zhang, X., Knorr, G., Lohmann, G. & Barker, S. Abrupt North Atlantic circulation changes in response to gradual CO_2 forcing in a glacial climate state. *Nat. Geosci.* **10**, 518–523 (2017).

46. Stouffer, R. J. & Manabe, S. Equilibrium response of thermohaline circulation to large changes in atmospheric CO_2 concentration. *Clim. Dyn.* **20**, 759–773 (2003).

47. Meehl, G. A. et al. Climate change projections in the 21st century and climate change commitment in the CCSM3. *J. Clim.* **19**, 2597–2616 (2006).

48. Meehl, G. A. et al. Climate system response to external forcings and climate change projections in CCSM4. *J. Clim.* **25**, 3661–3683 (2012).

49. Hu, A. et al. Effects of the Bering Strait closure on AMOC and global climate under different background climates. *Prog. Oceanogr.* **132**, 174–196 (2015).

50. Otto-Bliesner, B. L. et al. Changes in Arctic Gateways Amplify North Atlantic Warming in the Late Pliocene. *Geophys. Res. Lett.* **44**, 957–964 (2017).

51. Loulergue, L. et al. Orbital and millennial-scale features of atmospheric CH_4 over the past 800,000 years. *Nature* **453**, 383–386 (2008).

52. Peltier, W. R. Global glacial isostasy and the surface of the ice-age Earth: the ICE-5G (VM2) model and GRACE. *Annu. Rev. Earth Planet. Sci.* **32**, 111–149 (2004).

53. Petit, J. R. et al. Climate and atmospheric history of the past 420,000 years from the Vostok ice core, Antarctica. *Nature* **399**, 429–436 (1999).

Acknowledgements

Author contributions

A.H. designed and conducted the numerical model simulations and did the major analysis; A.A.-O. helped the design of experiments for mid-glacial conditions; G.A.M., W.H., B.O.-B., F.H., and T.W. contributed to the interpretation of the results; W.G.S., J.E., F.H., and N.R. helped with the model simulation setup and data processing. All have been actively involved in writing and refining the manuscript.

Competing interests

The authors declare no competing interests.

Additional information

Supplementary information The online version contains supplementary material available at https://doi.org/10.1038/s43247-023-00916-0.

Correspondence and requests for materials should be addressed to Aixue Hu.

Peer review information *Communications Earth & Environment* thanks Andreas Schmittner, Helene Hewitt and the other, anonymous, reviewer(s) for their contribution to the peer review of this work. Primary Handling Editors: Sze Ling Ho and Joe Aslin. A peer review file is available

Reprints and permission information is available at http://www.nature.com/reprints

Publisher's note Springer Nature remains neutral with regard to jurisdictional claims in published maps and institutional affiliations.